

# 1 **MUTATE: A Human Genetic Atlas of Multi-organ AI**

## 2 **Endophenotypes using GWAS Summary Statistics**

3  
4 Aleix Boquet-Pujadas<sup>1</sup>, Jian Zeng<sup>2</sup>, Ye Ella Tian<sup>3</sup>, Zhijian Yang<sup>4</sup>, Li Shen<sup>5</sup>, MULTI consortium<sup>#</sup>,  
5 Andrew Zalesky<sup>3</sup>, Christos Davatzikos<sup>6</sup>, Junhao Wen<sup>1\*</sup>,

6  
7 <sup>1</sup>Laboratory of AI and Biomedical Science (LABS), University of Southern California, Los Angeles, California,  
8 USA

9 <sup>2</sup>Institute for Molecular Bioscience, University of Queensland, Brisbane, QLD 4072, Australia

10 <sup>3</sup>Melbourne Neuropsychiatry Centre, Department of Psychiatry, Melbourne Medical School, The University of  
11 Melbourne, Melbourne, Victoria, Australia

12 <sup>4</sup>GE Healthcare, Bellevue, WA, USA

13 <sup>5</sup>Department of Biostatistics, Epidemiology and Informatics, University of Pennsylvania Perelman School of  
14 Medicine, Philadelphia, PA, USA

15 <sup>6</sup>Artificial Intelligence in Biomedical Imaging Laboratory (AIBIL), Center for AI and Data Science for Integrated  
16 Diagnostics (AI<sup>2</sup>D), Perelman School of Medicine, University of Pennsylvania, Philadelphia, USA

17  
18 \*Corresponding authors:

19 Junhao Wen, [junhao.wen89@gmail.com](mailto:junhao.wen89@gmail.com)

20 2025 Zonal Ave, Los Angeles, CA 90033, United States

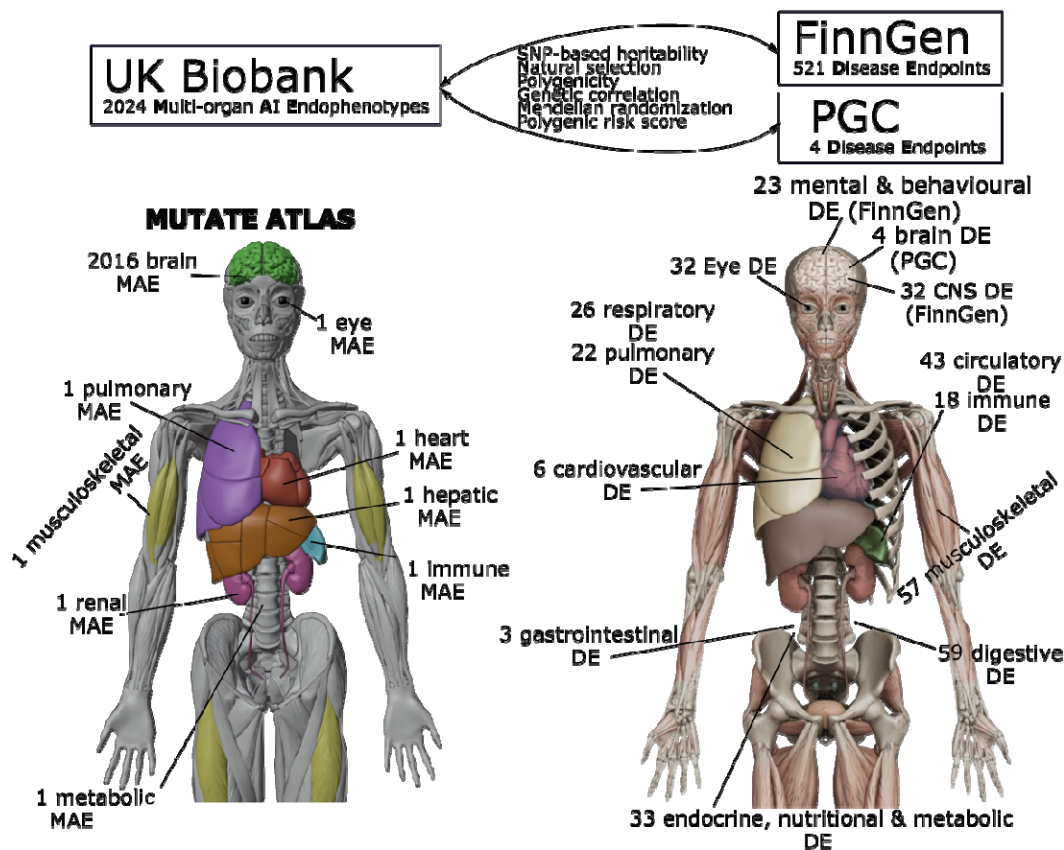
21 # Consortium representative: Dr. Junhao Wen

22

## 23 **Highlight**

- 24 • Two AI- and neuroimaging-derived subtypes of schizophrenia (MAE-SCZ1 and MAE-  
25 SCZ2) show lower polygenicity and weaker negative selection signatures than the disease  
26 endpoint/diagnosis of schizophrenia, supporting the endophenotype hypothesis.
- 27 • Brain AI endophenotypes are more polygenic than other organ systems.
- 28 • Most multi-organ AI endophenotypes exhibit negative selection signatures, whereas a  
29 small proportion of brain patterns of structural covariance networks exhibit positive  
30 selection signatures.
- 31 • The 2024 multi-organ AI endophenotypes are genetically and causally associated with  
32 within-organ and cross-organ disease endpoints/diagnoses.

### 33 Graphical abstract



34

35 **Keywords**

36 Multi-organ AI endophenotypes, genetic correlation, Mendelian randomization, polygenic risk  
37 score

38

## 39 **Summary**

40 Artificial intelligence (AI) has been increasingly integrated into imaging genetics to provide  
41 intermediate phenotypes (i.e., endophenotypes) that bridge the genetics and clinical  
42 manifestations of human disease. However, the genetic architecture of these AI endophenotypes  
43 remains largely unexplored in the context of human multi-organ system diseases. Using publicly  
44 available GWAS summary statistics from UK Biobank, FinnGen, and the Psychiatric Genomics  
45 Consortium, we comprehensively depicted the genetic architecture of 2024 multi-organ AI  
46 endophenotypes (MAEs). Two AI- and imaging-derived subtypes<sup>1</sup> showed lower polygenicity  
47 and weaker negative selection effects than schizophrenia disease diagnoses<sup>2</sup>, supporting the  
48 endophenotype hypothesis<sup>3</sup>. Genetic correlation and Mendelian randomization analyses reveal  
49 both within-organ relationships and cross-organ interconnections. Bi-directional causal  
50 relationships were established between chronic human diseases and MAEs across multiple organ  
51 systems, including Alzheimer's disease for the brain, diabetes for the metabolic system, asthma  
52 for the pulmonary system, and hypertension for the cardiovascular system. Finally, we derived  
53 polygenic risk scores for the 2024 MAEs for individuals not used to calculate MAEs and  
54 returned these to the UK Biobank. Our findings underscore the promise of the MAEs as new  
55 instruments to ameliorate overall human health. All results are encapsulated into the MUTATE  
56 genetic atlas and are publicly available at <https://labs-laboratory.com/mutate>.

## 57 Introduction

58 Multi-organ research<sup>1,4-11</sup> represents a pivotal frontier in advancing our understanding of human  
59 aging and disease. In particular, integrating artificial intelligence (AI) into multi-organ imaging  
60 genetics<sup>1,4,12,6</sup> has emerged as a novel approach, offering potential promise in advancing  
61 precision medicine<sup>13</sup>. This integration introduces a new array of endophenotypes<sup>14,15</sup>, serving as  
62 intermediate, often quantitative, phenotypes, potentially reshaping how we perceive and  
63 approach medical AI<sup>16</sup> in imaging and genetic research.

64 In recent years, three primary catalysts have significantly advanced the field of genetics.  
65 The first pivotal factor stems from the extensive collaborative efforts in consolidating large-scale  
66 multi-omics datasets, which has endowed researchers with unprecedented statistical power  
67 previously inaccessible. As an illustration, the UK Biobank (UKBB) study<sup>17</sup> stands out for its  
68 comprehensive collection of multi-organ imaging<sup>18</sup>, genetics<sup>19</sup>, and proteomics<sup>20,21</sup> data within  
69 the United Kingdom. Similarly, the FinnGen study<sup>22</sup>, conducted in Finland, has amassed  
70 extensive clinical and genetic data. Secondly, efforts toward open science have propelled the  
71 field, especially emphasizing the significance of publicly available resources, such as genome-  
72 wide association study (GWAS) summary statistics and widespread scientific dissemination.  
73 Notably, the FinnGen study and Psychiatric Genomics Consortium (PGC<sup>23</sup>) have publicly made  
74 all the GWAS summary statistics accessible<sup>22</sup>. Public GWAS platforms such as the GWAS  
75 Catalog<sup>24</sup>, OpenGWAS<sup>25</sup>, and GWAS ATLAS<sup>26</sup> have consolidated and harmonized vast GWAS  
76 datasets, rendering them suitable for subsequent genetic analyses. Likewise, such good practice  
77 was also employed in the newly burgeoning field of brain imaging genetics<sup>27</sup>, including the  
78 BIG40 (<https://open.win.ox.ac.uk/ukbiobank/big40/>), the BIG-KP (<https://bigkp.org/>),  
79 BRIDGEPORT (<https://labs-laboratory.com/bridgeport>), and MEDICINE (<https://labs-laboratory.com/medicine>)  
80 knowledge portals. Finally, advanced computational genomics  
81 statistical methods using solely GWAS summary statistics, along with sufficient linkage  
82 disequilibrium information, have been developed, presenting an unparalleled chance to  
83 comprehend the genetic architecture of highly polygenic disease traits. For example, LDSC<sup>28</sup> has  
84 been extensively utilized to estimate single-nucleotide polymorphism (SNP)-based heritability  
85 and genetic correlations. Mendelian randomization<sup>29</sup> is a statistical method to dissect associations  
86 further, probing potential causal relationships among these complex human disease traits,  
87 although these methods often rely on several sensitive model assumptions<sup>30</sup>.

88 Despite these advancements, the intricate genetic foundation shaping these AI  
89 endophenotypes in the context of pleiotropic human disease endpoints (DE) within multi-organ  
90 systems remains largely uncharted. We previously applied AI to imaging genetic data and  
91 derived 2024 multi-organ AI endophenotypes (MAE). These encompassed 2003 multi-scale  
92 brain patterns of structural covariance (PSC) networks generated through a deep learning-  
93 analogy non-negative matrix factorization method<sup>12</sup> (visualization for C32\_1 encompassing deep  
94 subcortical structures: [https://labs-laboratory.com/bridgeport/MuSIC/C32\\_1](https://labs-laboratory.com/bridgeport/MuSIC/C32_1)), 9 dimensional  
95 neuroimaging endophenotypes (DNE) quantifying neuroanatomical heterogeneity (also known as  
96 disease subtype) within 4 common brain diseases<sup>7</sup>, and 12 biological age gap (BAG) assessing  
97 the individual deviation in typical aging (i.e., acceleration or deceleration from the chronological  
98 age) across 9 human organ systems<sup>4,6</sup> (**Supplementary eTable 1a**). To contribute to open  
99 science<sup>31</sup>, we made all the GWAS summary statistics derived from UKBB data publicly  
100 available at the MEDICINE knowledge portal: <https://labs-laboratory.com/medicine>. In addition,  
101 FinnGen analyzed genetic data for 2269 binary and 3 quantitative DEs from 377,277 individuals  
102 and 20,175,454 variants. They made these massive GWAS summary statistics publicly available

103 to the community at <https://finngen.gitbook.io/documentation/> (**Supplementary eTable 1b**).  
104 Finally, PGC consolidated GWAS results focused on neurological disorders worldwide and  
105 made the GWAS summary statistics accessible to the research community (<https://pgc.unc.edu/>,  
106 **Supplementary eTable 1c**).

107 This study harnesses the extensive GWAS summary resources made publicly available  
108 by us on behalf of UKBB, FinnGen, and PGC (**Method 1**), along with the utilization of several  
109 advanced computational genomics statistical methods (refer to **Code Availability**), to thoroughly  
110 depict the genetic architecture of the 2024 MAEs (**Method 2**) and 525 DEs (>5000 cases) in the  
111 context of multi-organ investigations. Importantly, our previous research explored the genetic  
112 foundation of the 2024 MAEs but did not systematically encompass the FinnGen or PGC data.  
113 Specifically, we included 521 DEs released by the FinnGen study, accessible at  
114 <https://finngen.gitbook.io/documentation/v/r9/>, and 4 brain DEs (Alzheimer’s disease (AD),  
115 Attention-deficit/hyperactivity disorder (ADHD), bipolar disorder (BIP), and schizophrenia  
116 (SCZ)) from PGC (<https://pgc.unc.edu/>). This study expanded on this by systematically  
117 benchmarking the genetic analyses and comprehensively comparing various statistical  
118 methodologies<sup>28,30,32–38</sup> (**Method 3**). Specifically, we aimed to compute the SNP-based  
119 heritability ( $h_{SNP}^2$ ), polygenicity ( $\pi$ ), the relationship between SNP effect size and minor allele  
120 frequency ( $S$ : signature of natural selection, genetic correlation ( $r_g$ ), causality, and polygenic risk  
121 score (PRS) between the 2024 MAEs and 525 DEs. These findings were encapsulated within the  
122 MUTATE (**MU**Ti-organ **AI** endopheno**TypE**) genetic atlas, which is publicly available at  
123 <https://labs-laboratory.com/mutate>.

## 124 Results

### 125 The genetic architecture of the 2024 MAEs and 525 DEs

126 We computed three parameters to fully depict the genetic architecture of the 2024 MAEs  
127 (**Method 3a**). For the SNP-based heritability ( $h_{SNP}^2$ ), SBayesS<sup>39</sup> obtained the highest  $h_{SNP}^2$  for the  
128 2016 brain MAEs (mean  $\hat{h}_{SNP}^2=0.13$  [0.01, 0.38]), followed by the pulmonary BAG  
129 ( $0.16\pm 0.004$ ), the eye BAG ( $0.14\pm 0.009$ ), the cardiovascular BAG ( $0.12\pm 0.003$ ), the renal BAG  
130 ( $0.10\pm 0.003$ ), and the musculoskeletal BAG ( $0.10\pm 0.003$ ) (**Fig. 1a** and **Supplementary eFile 1**).  
131 It is worth noting that SNP-based heritability varies across methods and depends on the input  
132 data, i.e., summary data or individual-level genotype data used in the method<sup>40</sup>. We aimed to  
133 benchmark the summary data-based methods by comparing the results from SBayesS with those  
134 of LDSC<sup>28</sup> and SumHer<sup>33</sup>. Overall, while the estimates from the three methods were highly  
135 correlated ( $r=0.97$  between LDSC and SumHer;  $r=0.99$  between SBayesS and SumHer;  $r=0.99$   
136 between SBayesS and LDSC; **Supplementary eFigure 1**), SumHer ( $0.23\pm 0.14$ ) generally  
137 yielded larger  $h_{SNP}^2$  estimates than both LDSC ( $0.16\pm 0.10$ ) and SBayesS ( $0.13\pm 0.08$ )  
138 (**Supplementary eFile 1**). We present the  $h_{SNP}^2$  estimate of the 525 DEs and 2024 MAEs in  
139 **Supplementary eFigure 2**. **Supplementary eFile 2** presents the results of the 525 DEs. For the  
140 525 DEs, we converted the  $h_{SNP}^2$  estimates from the observed scales to the liability scales,  
141 following the recommendations of Ojavee et al<sup>41</sup>. It's important to clarify that we did not intend  
142 to compare the  $h_{SNP}^2$  estimates of the two data sources due to differences in genotype coverage,  
143 sample sizes, allele frequencies, and other factors.

144 We then computed the natural selection signature ( $S$ ) for the 2024 MAEs. The metabolic  
145 BAG showed a strong negative selection ( $S=-0.82\pm 0.10$ ), followed by the pulmonary BAG ( $S=-$   
146  $0.79\pm 0.05$ ), the hepatic BAG ( $S=-0.74\pm 0.09$ ), the renal BAG ( $S=-0.68\pm 0.08$ ), and the immune  
147 BAG ( $S=-0.66\pm 0.11$ ). For the brain MAEs ( $S=-0.33$  [-1, 0.43]), the brain BAG and ( $S=-$   
148  $0.70\pm 0.12$ ) the subtype (ASD1) for autism spectrum disorder<sup>42</sup> ( $S=-0.90\pm 0.11$ ) showed strong  
149 negative selection effects (**Fig. 1b** and **Supplementary eFile 3**).

150 Finally, we calculated the polygenicity ( $\pi$ ) for the 2024 MAEs. We found that brain  
151 MAEs ( $0.040$  [0.003, 0.072]) showed higher polygenicity than other organ systems (t-  
152 statistic=5.75; P-value= $1.03\times 10^{-8}$ ), followed by the pulmonary BAG ( $0.018\pm 0.001$ ), the  
153 musculoskeletal BAG ( $0.013\pm 0.001$ ), and the cardiovascular BAG ( $0.011\pm 0.001$ ) (**Fig. 1C** and  
154 **Supplementary eFile 4**). The PSC (C128\_115: [https://labs-](https://labs-laboratory.com/bridgeport/MuSIC/C128_115)  
155 [laboratory.com/bridgeport/MuSIC/C128\\_115](https://labs-laboratory.com/bridgeport/MuSIC/C128_115)) showed the highest polygenicity estimate  
156 ( $0.072\pm 0.002$ ).

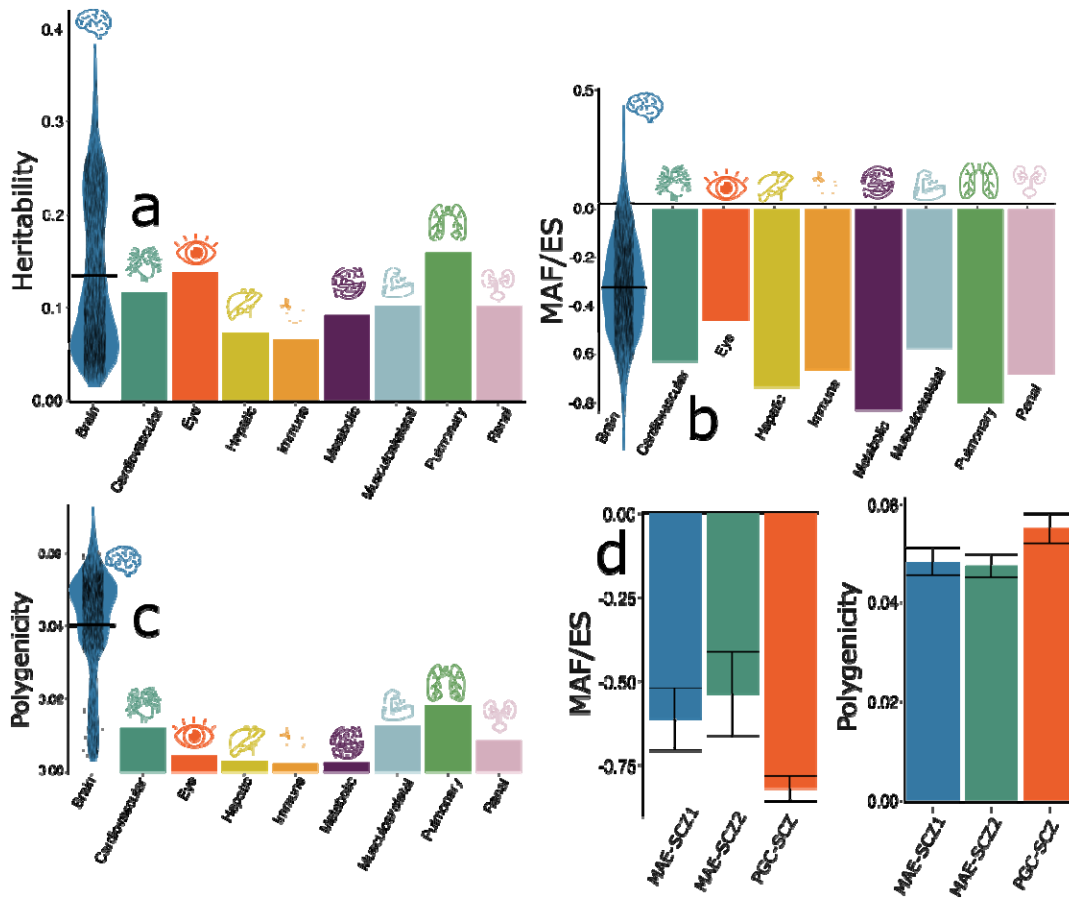
157

### 158 Potential evidence for the endophenotype hypothesis

159 Previous studies<sup>43,44</sup> have found supporting evidence for the endophenotype hypothesis<sup>14,15</sup> using  
160 traditional brain map-based signatures, showing that more genetic variants are associated with  
161 disease endpoints than imaging-derived signatures (i.e., endophenotypes). Of note, considering  
162 genetic differences between FinnGen and UKBB samples, SBayesS with the UKBB as LD  
163 reference may give biased estimates of  $S$  and  $\pi$  (LD from FinnGen not fully available; **Method**  
164 **3a**). Therefore, we used the GWAS summary data for PGC schizophrenia (SCZ<sup>2</sup>) and two  
165 subtypes of SCZ (SCZ1 and SCZ2<sup>1</sup>) from our UKBB analysis to demonstrate this. The  
166 advantage of using PGC data is that the GWAS summary statistics are better powered (large  
167 sample sizes), and the data were from European ancestry groups across different countries. A  
168 data harmonization procedure is outlined in **Supplementary eMethod 1** to ensure a fair



169 comparison of these estimates, which led to the utilization of a common set of SNPs and linkage  
 170 disequilibrium information for computing the  $S$  and  $\lambda$  parameters. Our results showed that MAE-  
 171 SCZ1 ( $\lambda = -0.048 \pm 0.002$ ;  $S = -0.61 \pm 0.09$ ) and MAE-SCZ2 ( $\lambda = -0.047 \pm 0.002$ ;  $S = -0.54 \pm 0.12$ ) had  
 172 lower polygenicity signals and weaker negative selection effects than PGC-SCZ  
 173 ( $\lambda = -0.055 \pm 0.003$ ;  $S = -0.82 \pm 0.04$ ) (**Fig. 1d**). **Supplementary eFigure 3** shows the Manhattan plot  
 174 of the harmonized summary data for MAE-SCZ1, MAE-SCZ2, and PGC-SCZ. These findings  
 175 potentially support the endophenotype hypothesis<sup>3</sup>, which suggests that intermediate phenotypes  
 176 (e.g., SCZ subtype MAEs) reside inside the causal pathway from genetics to exo-phenotypes  
 177 (e.g., SCZ binary diagnosis), making them closer to the underlying etiology<sup>43,44</sup>.



178  
 179 **Figure 1: The genetic architecture of the 2024 MAEs**

180 Three parameters are estimated by SBayesS to delineate the genetic architecture of the 2024  
 181 MAEs, including (a) the SNP-based heritability ( $h^2$ ), (b) the relationship between MAF and  
 182 effect size ( $S$ ), and (c) polygenicity ( $\lambda$ ). (d) We compared the  $\lambda$  and  $S$  parameters using  
 183 harmonized GWAS summary data for two AI- and imaging-derived subtypes (MAE-SCZ1 and  
 184 MAE-SCZ2<sup>1</sup>) from UKBB and the disease endpoint of schizophrenia (PGC-SCZ<sup>2</sup>) from PGC.  
 185 FinnGen data was not used due to bias stemming from the unavailability of FinnGen-specific  
 186 linkage disequilibrium data (**Supplementary eMethod 1**). We present the distribution of the  
 187 estimated parameters for the 2016 brain MAEs using a violin plot; the mean value is denoted by  
 188 the black horizontal line. These results should be interpreted cautiously for comparative purposes  
 189 due to limitations stemming from the lack of individual genotype data from FinnGen and PGC,  
 190 differing linkage disequilibrium structures, and varying sample sizes.

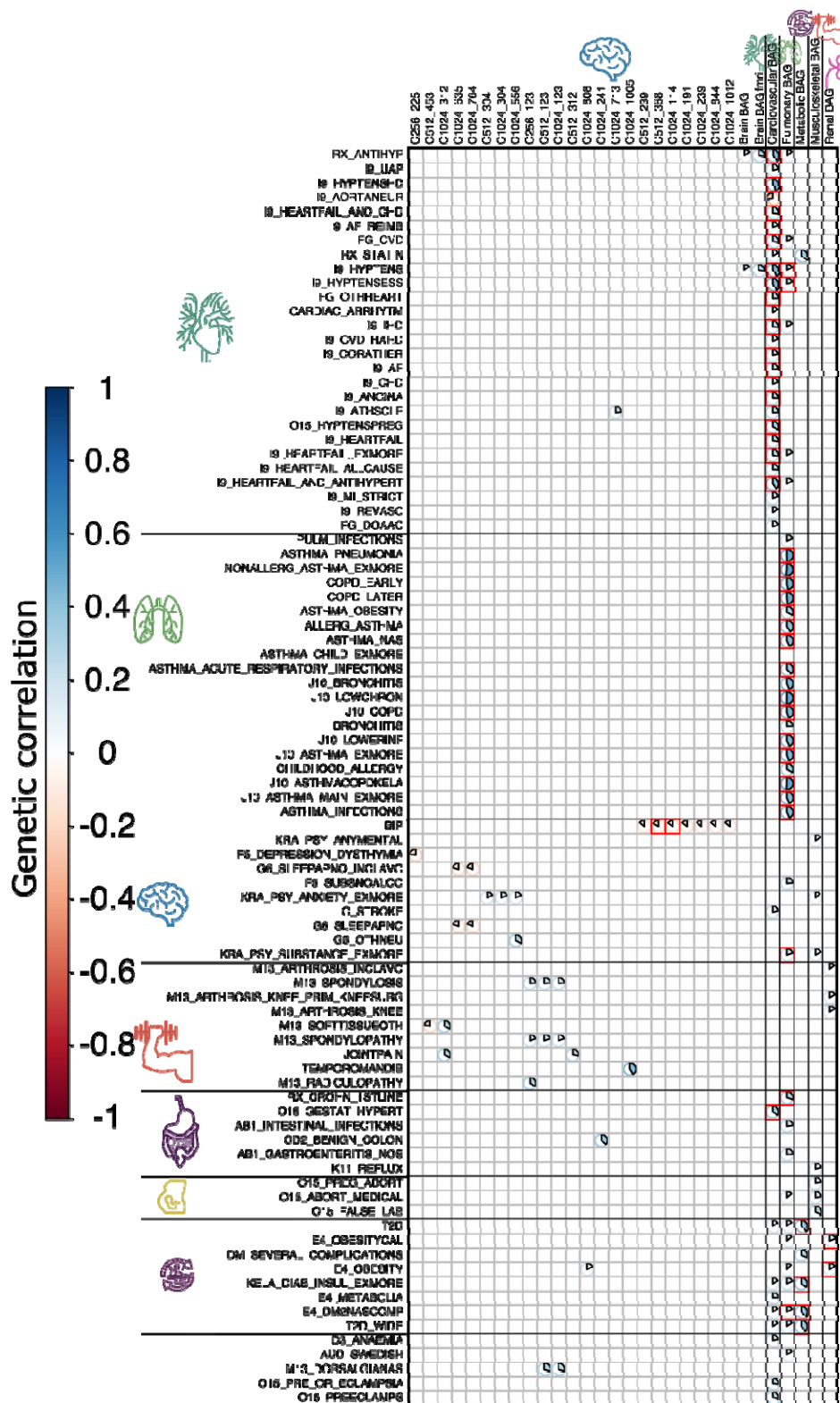
191

192 **The genetic correlation shows organ-specific and cross-organ associations**

193 We found 132 (P-value < 0.05/2024) and 45 (P-value < 0.05/2024/525) commonly significant  
194 positive genetic correlations ( $r_g$ ) after applying two levels of Bonferroni correction (**Fig. 2**) for  
195 the LDSC<sup>28</sup> and GNOVA<sup>34</sup> methods (**Method 3b**, **Supplementary eFile 5**, and **Supplementary**  
196 **eTable 2**). We noted that HDL encountered convergence issues with the models, as detailed in  
197 **Method 3b**.

198 Between these methods, the magnitude of the genetic correlations for the significant  
199 signals for both methods differed: mean  $\hat{r}_g=0.24[-0.40\sim0.52]$  with 213 significant signals for  
200 LDSC, mean  $\hat{r}_g=0.17[-0.30\sim0.62]$  for GNOVA with 428 significant signals (**Fig. 2**). The three  
201 sets of converged estimates showed a strong correlation:  $r=0.77$  (P-value< $1\times10^{-10}$ ;  $N=1,062,577$ )  
202 between LDSC and GNOVA,  $r=0.81$  (P-value< $1\times10^{-10}$ ;  $N=59,289$ ) between LDSC and HDL,  
203 and  $r=0.82$  (P-value< $1\times10^{-10}$ ;  $N=59,289$ ) between GNOVA and HDL. **Supplementary eFigure**  
204 **4** shows the correlation of the three sets of estimates.

205 Within the significant signals identified, we observed *i*) organ-specific associations, in  
206 which the MAE showed a genetic association with the DE originating from the respective organ  
207 system, and *ii*) cross-organ connections, in which the MAE and DE were primarily involved  
208 from different organ systems. For example, two brain PSCs showed significant negative genetic  
209 correlations with BIP from PGC (C512\_368 vs. BIP:  $-0.16\pm0.03$ ; C1024\_114 vs. BIP:  $-$   
210  $0.15\pm0.03$ ). At a less stringent level, the brain MAEs were also genetically associated with DEs  
211 from other organ systems, including the positive correlation between C1024\_808 and obesity  
212 (E4\_OBESITY:  $r_g=0.17\pm0.13$ ). The cardiovascular BAG was positively correlated with several  
213 DEs related to the cardiovascular system, including ischemic heart disease (I9\_IHD:  
214  $r_g=0.26\pm0.03$ ), coronary heart disease (I9\_HEARTFAIL\_AND\_CHD:  $r_g=0.26\pm0.03$ ), angina  
215 (I9\_ANGINA:  $r_g=0.25\pm0.03$ ) and atrial fibrillation (I9\_Af:  $r_g=0.22\pm0.04$ ). Likewise, the  
216 pulmonary BAG was positively associated with multiple DEs related to the lung and respiratory  
217 system, including chronic obstructive pulmonary disease (COPD\_EARLY:  $r_g=0.47\pm0.04$ ) and  
218 various forms of asthma (ASTHMA\_NAS:  $r_g=0.43\pm0.04$ ). Cross-organ connections were  
219 established, such as between the pulmonary BAG and substance abuse  
220 (KRA\_PSY\_SUBSTANCE\_EXMORE:  $r_g=0.20\pm0.03$ ) and hypertension (I9\_HYPTENS:  
221  $r_g=0.17\pm0.03$ ). Lastly, the metabolic BAG was largely linked to different forms of diabetes  
222 (T2D:  $r_g=0.40\pm0.04$ ).



223  
 224 **Figure 2: Genetic correlation between the 2024 MAEs and 525 DEs**  
 225 The significant genetic correlation estimates ( $r_g$ ) between 2024 MAEs and 525 DEs are depicted,  
 226 considering two levels of corrections for multiple comparisons, considering the relatively smaller  
 227 sample sizes (<40,000) for brain MAEs compared to other organ MAEs (>100,000). Initially, we

228 reveal significant results shared between LDSC and GNOVA, employing Bonferroni correction  
229 based solely on the number of MAEs (P-value<0.05/2024), uncovering 133 MAE-AE pairs.  
230 Subsequently, a stricter correction based on both the number of MAEs and DEs is applied,  
231 leading to 45 unique MAE-AE pairs marked as red squares; the numeric results are displayed  
232 using results from LDSC. The genetic correlation for non-significant results was set to 0 for  
233 visualization purposes. For the MAEs, readers can explore the BRIDGEPORT portal for a visual  
234 representation of the 2003 brain PSCs (e.g., C256\_225: [https://labs-](https://labs-laboratory.com/bridgeport/MuSIC/C256_225)  
235 [laboratory.com/bridgeport/MuSIC/C256\\_225](https://labs-laboratory.com/bridgeport/MuSIC/C256_225)) and the other BAGs at the MEDICINE portal:  
236 <https://labs-laboratory.com/medicine>.

### 237 238 **The brain, cardiovascular, and pulmonary MAEs are causally linked to DEs of multiple** 239 **organ systems**

240 Employing five distinct two-sample Mendelian randomization estimators, we identified 39 (P-  
241 value<0.05/633) and 15 (P-value<0.05/633/524) significant causal relationships, directed from  
242 the MAE to DE, that withstood the Bonferroni correction at two different levels of rigors, as per  
243 the inverse variance weighted (IVW) estimator and at least one of the other four estimators  
244 (**Method 3c** and **Supplementary eTable 3**).

245 Within the 15 significant causal relationships, the brain MAEs showed causal  
246 connections with DEs from the brain, as well as DEs from other organ systems. For example, the  
247 brain PSC (C1024\_598) was causally linked to SCZ from PGC [P-value=9.89x10<sup>-8</sup>; OR (95%  
248 CI)=0.69 (0.59, 0.79); the number of IVs=7]. C1024\_684 was causally linked to Ventral hernia  
249 from FinnGen [K11\_VENTHER: P-value=1.09x10<sup>-7</sup>; OR (95% CI)=1.43 (1.25, 1.63); the  
250 number of IVs=18]. The pulmonary BAG was causally linked to multiple DEs related to the  
251 pulmonary system, including chronic obstructive pulmonary disease (COPD) [J10\_COPD: P-  
252 value=2.70x10<sup>-20</sup>; OR (95% CI)=1.77 (1.56, 2.00); the number of IVs=59] and asthma  
253 [ASTHMA\_PNEUMONIA: P-value=1.51x10<sup>-14</sup>; OR (95% CI)=1.67 (1.41, 1.96); the number of  
254 IVs=59]. The cardiovascular BAG was causally linked to ischemic heart disease (IHD)  
255 [ASTHMA\_PNEUMONIA: P-value=1.09x10<sup>-7</sup>; OR (95% CI)=1.64 (1.36, 1.96); the number of  
256 IVs=37] (**Fig. 3**). The quality check of the significant signals is presented in **Supplementary**  
257 **eFolder 1. Supplementary eFile 6** presents the full set of results for the 521 FinnGen DEs and 4  
258 PGC DEs.

259  
260

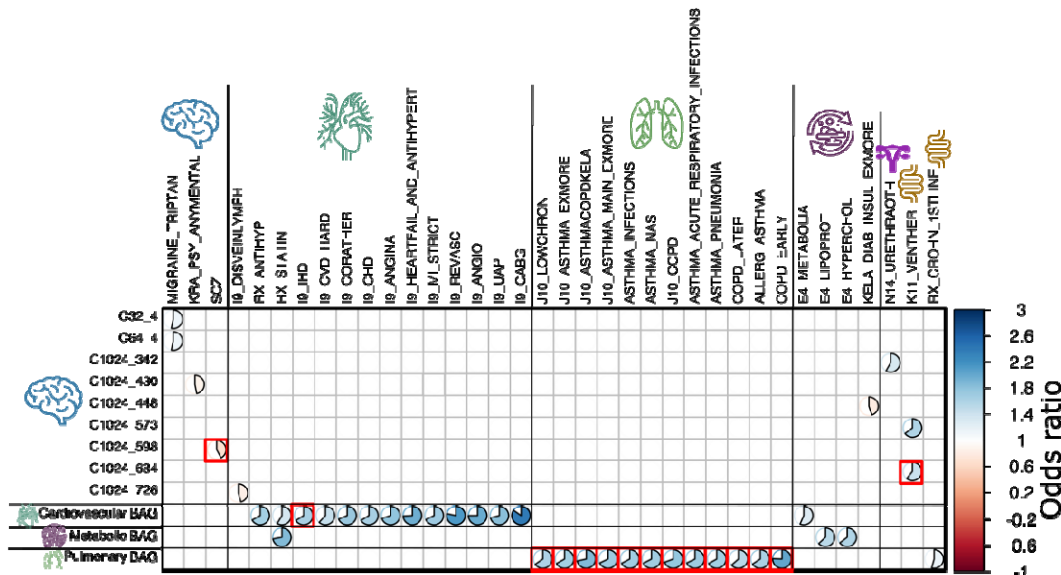


**Figure 3: Causal relationship from the 2024 MAEs to the 525 DEs**

The causal relationship from the 2024 MAEs to the 525 DEs revealed 39 significant MAE-DE pairs, involving 633 MAEs as effective exposure variables (>8 instrumental variables before harmonization) and 525 DEs as outcomes. Bonferroni correction was applied to identify potential significant causal signals based on *i*) the 633 MAEs ( $P\text{-value} < 0.05/633$ ) and *ii*) the 633 MAEs and 525 DEs ( $P\text{-value} < 0.05/633/524$ , denoted by the 15 red rectangles). Furthermore, we verified that the statistical significance attained for the IVW estimator was consistent and persisted across at least one of the other four Mendelian randomization estimators (Egger, weighted median, simple mode, and weighted mode estimators). For visualization purposes, the odds ratios for non-significant results were set to 1 and were left blank. For the MAEs, readers can explore the BRIDGEPORT portal for a visual representation of the 2003 brain PSCs (e.g., C32\_4: [https://labs-laboratory.com/bridgeport/MuSIC/C32\\_4](https://labs-laboratory.com/bridgeport/MuSIC/C32_4)) and the other BAGs at the MEDICINE portal: <https://labs-laboratory.com/medicine>.

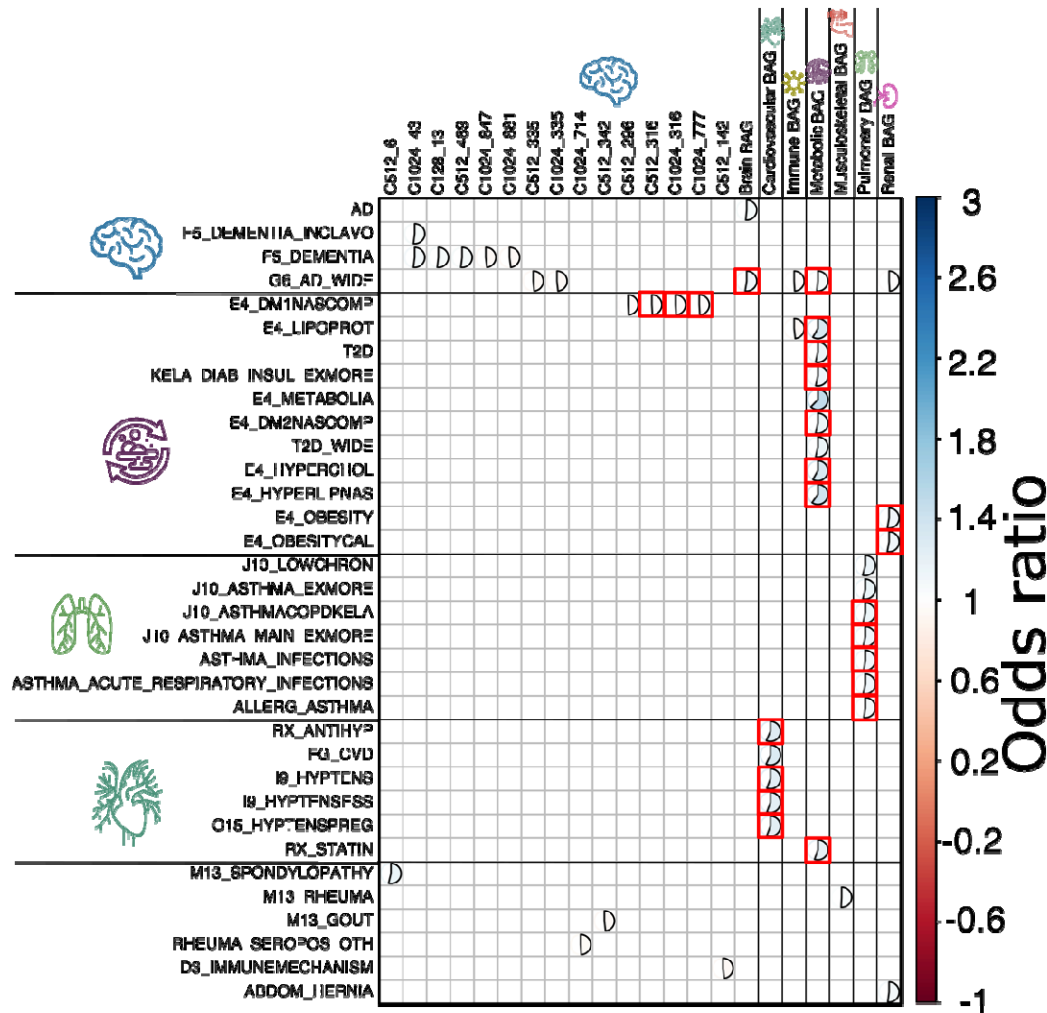
### The DEs involving Alzheimer’s disease, diabetes, asthma, and hypertension exert causal effects on multi-organ MAEs

We then tested the inverse causality by employing the DEs as exposure and MAEs as outcome variables. We identified 47 ( $P\text{-value} < 0.05/787$ ) and 23 ( $P\text{-value} < 0.05/787/214$ ) significant causal relationships, directed from the DE to MAE, that survived the Bonferroni correction at two different levels of rigors (**Method 3c** and **Supplementary eTable 4**).

Within the 23 significant causal relationships ( $P\text{-value} < 0.05/787/214$ ), various forms of Alzheimer’s disease were linked to the brain MAEs, including the brain BAG [G6\_AD\_WIDE:  $P\text{-value} = 3.03 \times 10^{-7}$ ; OR (95% CI) = 1.10 (1.06, 1.13); the number of IVs = 8] and metabolic BAG [G6\_AD\_WIDE:  $P\text{-value} = 3.03 \times 10^{-7}$ ; OR (95% CI) = 1.07 (1.04, 1.09); the number of IVs = 8]. Type 1 diabetes (E4\_DM1NASCOMP) was also causally linked to multiple brain PSCs. In addition, the cardiovascular BAG was causally linked to multiple heart diseases, including hypertension [I9\_HYPTENS:  $P\text{-value} = 4.67 \times 10^{-31}$ ; OR (95% CI) = 1.23 (1.19, 1.27); the number of IVs = 110]. Several forms of asthma were causally linked to the pulmonary BAG, such as allergic asthma [ALLERG\_ASTHMA:  $P\text{-value} = 2.38 \times 10^{-9}$ ; OR (95% CI) = 1.09 (1.06, 1.13); the number of IVs = 14]. Finally, obesity was also linked to the renal BAG [E4\_OBESITY:  $P\text{-value} = 2.74 \times 10^{-8}$ ; OR (95% CI) = 1.11 (1.07, 1.15); the number of IVs = 19] (**Fig. 4**).



293 **Supplementary eFolder 2** presents the quality check results of the significant signals.  
 294 **Supplementary eFile 7** presents the full set of results for the 521 FinnGen DEs and 4 PGC DEs.  
 295



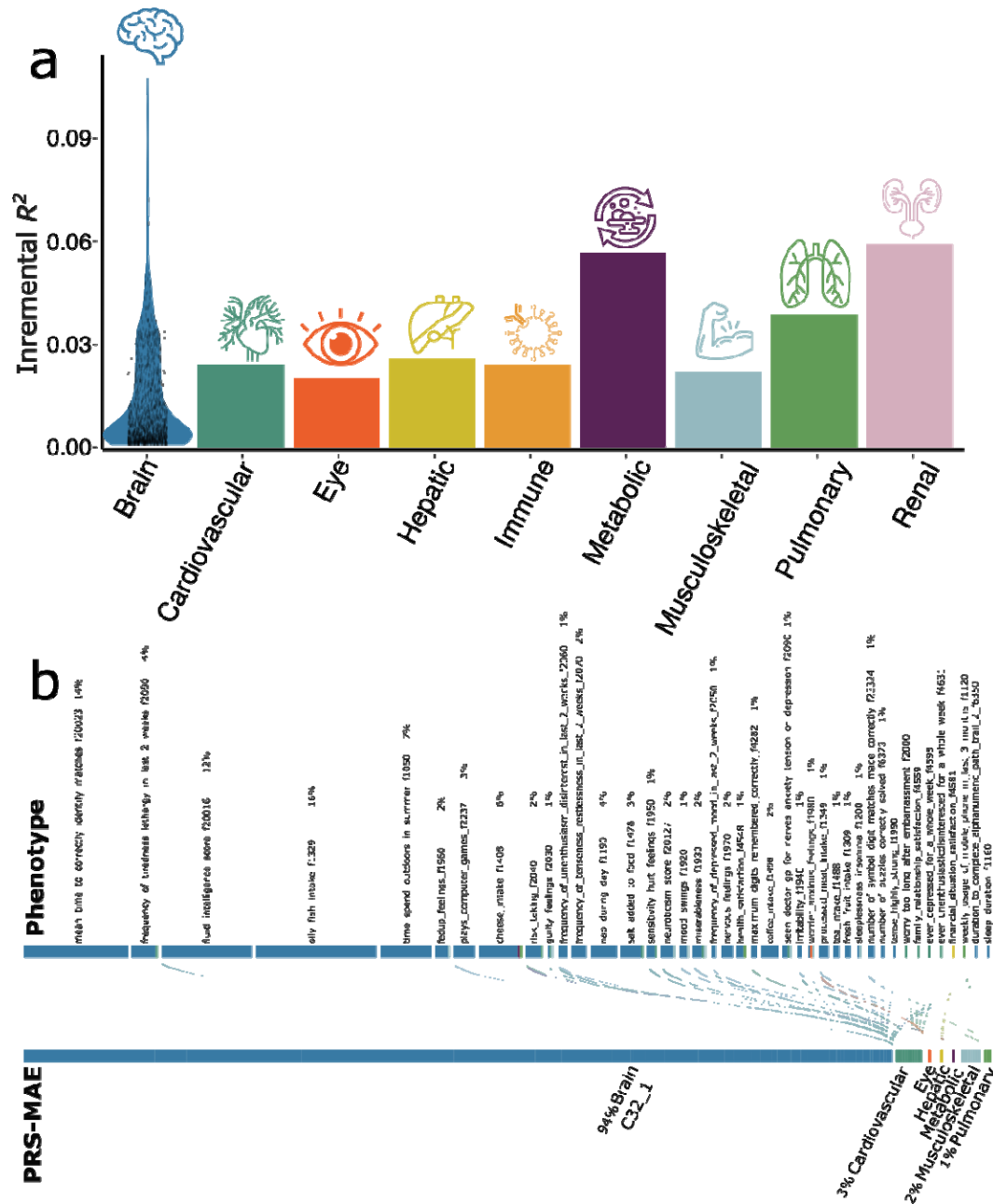
296 **Figure 4: Causal relationship from the 525 DEs to the 2024 MAEs**  
 297 The causal relationship from the 525 MAEs to the 2024 DEs revealed 47 significant DE-MAE  
 298 pairs, involving 214 DEs as effective exposure variables (>8 instrumental variables before  
 299 harmonization) and 787 DEs as effective outcomes after quality checks. Bonferroni correction  
 300 was applied to identify potential significant causal signals based on *i*) the 787 MAEs (P-  
 301 value<0.05/787) and *ii*) the 787 MAEs and 214 DEs (P-value<0.05/787/214, denoted by the 23  
 302 red rectangles). Furthermore, we verified that the statistical significance attained for the IVW  
 303 estimator was consistent and persisted across at least one of the other four Mendelian  
 304 randomization estimators (Egger, weighted median, simple mode, and weighted mode  
 305 estimators). For visualization purposes, the odds ratios for non-significant results were set to 1  
 306 and were left blank. For the MAEs, readers can explore the BRIDGEPORT portal for a visual  
 307 representation of the 2003 brain PSCs (e.g., C128\_13: [https://labs-](https://labs-laboratory.com/bridgeport/MuSIC/C128_13)  
 308 [laboratory.com/bridgeport/MuSIC/C128\\_13](https://labs-laboratory.com/bridgeport/MuSIC/C128_13)) and the other BAGs at the MEDICINE portal:  
 309 <https://labs-laboratory.com/medicine>.  
 310  
 311

312 **The polygenic risk scores of the 2024 MAEs**

313 Using the PRS-CS<sup>45</sup> method, we derived the PRS of the 2024 MAEs. We found that the 1799  
314 MAEs could significantly (P-value<0.05/2024) predict the phenotypic BAGs in the test/target  
315 data (split2 GWAS; detailed in **Method 3d**). Among these, 1791 brain MAEs resulted in  
316 significant incremental  $R^2$  ranging from 0.11% to 10.70% to predict the phenotype of interest.  
317 For example, the PSC (C1024\_593 for part of the cerebellum: [https://labs-  
318 laboratory.com/bridgeport/MuSIC/C1024\\_593](https://labs-laboratory.com/bridgeport/MuSIC/C1024_593)) showed an incremental of  $R^2$  10.70%. The renal  
319 BAG showed an incremental  $R^2$  of 5.92%, followed by the metabolic ( $R^2 = 5.67%$ ) and  
320 pulmonary BAG ( $R^2 = 3.86%$ ) (**Fig. 5a** and (**Supplementary eFile 8**)).

321 We then applied the model to the entire UKBB population and performed a PRS-wide  
322 association study (PWAS), where the 2024 PRS-MAEs were linked to the 59 phenotypes that  
323 were not initially used to compute the respective PRS, to avoid the circular bias<sup>46</sup>  
324 (**Supplementary eTable 5**). Refer to **Method 3d** for details. We found 388 significant  
325 associations (P-value<0.05/2024/59) between 7 PRS-MAEs and 41 phenotypes. Among these,  
326 PSC C32\_1 showed the most associations (94%); the lifestyle factor for only fish intake (Field  
327 ID: 16) was highly linked to multiple PRS-MAEs (16%). These results were expected because  
328 the 59 phenotypes (e.g., cognitive and mental traits) are primarily linked to the brain, and  
329 lifestyle factors were largely linked to multiple organ systems (**Fig. 5b** and **Supplementary  
330 eFile 9**). All derived PRS will be returned to UKBB and made available to the community.

331  
332



333  
 334 **Figure 5: The polygenic risk score of the 2024 MAEs and PWAS**  
 335 (a) The incremental  $R^2$  of the PRS derived by PRC-CS to predict the 2024 MAEs in the  
 336 target/test data (i.e., the split2 GWAS). The y-axis indicates the proportions of phenotypic  
 337 variation that the PRS can significantly and additionally explain (i.e., incremental  $R^2$ ). The x-axis  
 338 lists the 8 organ systems. For the brain, we showed the PRS distribution of the significant results  
 339 from the 1791 brain PRS-MAEs; the other organ systems only have one PRS-MAE. (b) The  
 340 PWAS links the PRS-MAEs to the 59 additional phenotypes not used to compute the PRS-MAE  
 341 in the entire UKBB sample ( $P$ -value $<0.05/2024/59$ ).  
 342



## 343 Discussion

344 This study expands previously established genetic atlases<sup>47,32</sup> by integrating AI-derived  
345 endophenotypes via the 2024 MAEs within the multi-organ framework solely through GWAS  
346 summary statistics. We demonstrate a promising avenue for advancing imaging genetic research  
347 in two key aspects: *i*) integrating AI in imaging genetics and *ii*) exploring human aging and  
348 disease through a multi-organ perspective.

349 By comprehensively depicting the genetic architecture of the 2024 MAEs, we showcased  
350 that AI endophenotypes supported the endophenotype hypothesis<sup>14,15</sup>, in which they showed  
351 lower polygenicity and weaker negative selection effects than the disease diagnosis. First, it may  
352 suggest that these intermediate phenotypes exist along the causal pathway, bridging the gap  
353 between underlying genetics and "exo-phenotypes" like cognitive decline or disease diagnoses in  
354 case/control studies, thus positioned closer to the core etiology and pathology. Secondly, many  
355 of these 2024 MAEs originated from *in vivo* imaging methodologies like magnetic resonance  
356 imaging (MRI). Consequently, they tend to exhibit reduced noise levels (i.e., a higher SNR) in  
357 capturing disease-related effects and are less susceptible to biases, such as misclassification<sup>48</sup>,  
358 case/control-covariate sample bias (e.g., studies matching comorbidities and other factors), and  
359 imbalanced case/control ratios, as evidenced in many GWASs in FinnGen. Especially for the  
360 former, binary traits have a threshold for disease classification, leading to the dichotomization of  
361 individuals into affected and unaffected categories. Thirdly, the 525 DEs often represent  
362 complex diseases highly influenced by multiple genetic and environmental factors. Their  
363 multifaceted nature, involving numerous genes with modest effects and environmental  
364 interactions<sup>49</sup>, can lead to a higher vulnerability to disease onset and clinical symptoms.  
365 Consistent with this observation, we previously also found that one AI- and imaging-derived  
366 subtype of Alzheimer's disease<sup>50</sup> (AD1), but not the binary disease diagnosis, was genetically  
367 correlated with brain age (GM- and WM-BAG)<sup>6</sup>.

368 We observed that brain MAEs were overall more polygenic than MAEs from other organ  
369 systems. Brain disorders are highly polygenic<sup>51</sup>. First, the brain is a highly complex organ with  
370 intricate functions, and disorders affecting it are likely influenced by a larger number of genetic  
371 variants<sup>12,52</sup>. Second, many brain disorders are multifaceted, involving various aspects of brain  
372 structure, function, and connectivity, which can be influenced by various genetic factors<sup>19</sup>.  
373 Additionally, the brain regulates many physiological processes throughout the body, so  
374 disruptions in its function can have widespread effects, potentially involving interactions with  
375 multiple organ systems<sup>4</sup>. In addition, we found that most of the brain MAEs showed negative  
376 selection signatures, including the 9 disease subtype DNEs and 4 brain BAGs; some of the brain  
377 PSCs showed a positive *S* estimate (e.g., for the occipital lobe and subcortical structure,  
378  $S=0.31\pm 0.09$ : [https://labs-laboratory.com/bridgeport/MuSIC/C32\\_18](https://labs-laboratory.com/bridgeport/MuSIC/C32_18)). The anticipated negative  
379 selection signatures of biological age across multiple organs and disease subtypes are expected to  
380 align with our prior findings, which revealed pervasive signatures of natural selection across a  
381 range of complex human traits and functional genomic categories. This negative selection  
382 signature prevents mutations with large deleterious effects from becoming frequent in the  
383 population<sup>53</sup>. The positive selection signatures identified in certain brain PSCs may suggest that  
384 positive selection may also play a role in shaping the genetic architecture of brain structural  
385 networks.

386 The MUTATE atlas uncovered both established and previously undiscovered interactions  
387 concerning human systemic diseases within individual organs and across diverse organ systems.  
388 For example, within the cardiovascular system, the AI-derived MAE, cardiovascular BAG

389 showed both substantial genetic correlation (**Fig. 2**) and bi-directional causality (**Fig. 3 and 4**)  
390 with multiple heart diseases, such as ischaemic heart disease<sup>54</sup>, heart failure<sup>55</sup>, and atrial  
391 fibrillation<sup>56</sup>. Similarly, pulmonary BAG was also causally linked to multiple diseases related to  
392 the lung and respiratory system, including COPD<sup>57</sup> and various forms of asthma<sup>58</sup>. Another  
393 organ-specific connection was observed in neurologic diseases, encompassing conditions such as  
394 AD<sup>59</sup> and various mental disorders<sup>60</sup> linked to several MAEs associated with the brain, notably  
395 several PSCs and WM-BAG. Cross-organ interplay was evidenced for several novel  
396 connections. For instance, the brain PSCs exhibited causal connections to conditions extending  
397 beyond the brain, such as ventral hernia and vein diseases, as well as systemic conditions, like  
398 various forms of diabetes affecting the entire body. In contrast, AD appears to causally impact  
399 multiple BAGs across various human organ systems, including the renal, immune, and metabolic  
400 systems. It's widely recognized that AD, being a complex condition, triggers detrimental effects  
401 that influence several human organ systems<sup>59,61</sup>. Our previous study used imaging genetics to  
402 investigate this multi-organ involvement along the disease continuum<sup>62</sup>. These results highlight  
403 the clinical relevance and interpretation of these AI endophenotypes to quantify individual-level  
404 organ health.

405 Emphasizing preventative strategies for specific chronic diseases is crucial to enhancing  
406 overall multi-organ health. Our MAEs present opportunities as novel instruments for selecting  
407 populations in clinical trials and facilitating therapeutic development. AD and various forms of  
408 diabetes exemplify disease endpoints significantly impacting multiple human organ systems. AD  
409 stands as the leading cause of dementia in older adults, presenting a persistent challenge in  
410 medicine despite numerous pharmacotherapeutic clinical trials. These trials have included  
411 interventions, such as anti-amyloid drugs<sup>63,64</sup> and anti-tau drugs<sup>65</sup>. The complexity and  
412 multifaceted nature of the underlying neuropathological processes may account for the lack of  
413 effective treatments. We call on the scientific community to embrace various mechanistic  
414 hypotheses to elucidate AD pathogenesis beyond amyloid and tau<sup>66,67</sup>. Likewise, the complexity  
415 of diabetes, with its various contributing factors, renders prevention challenging<sup>68</sup>. Moreover,  
416 diabetes often coexists with other chronic conditions affecting multiple organ systems, such as  
417 cardiovascular diseases, hypertension, and dyslipidemia<sup>69</sup>. Successful prevention strategies  
418 require a holistic approach, encompassing lifestyle adjustments, education, healthcare access,  
419 and societal considerations.

420

## 421 **Limitation**

422 This study presents several limitations. Primarily, our analyses were centered solely on GWAS  
423 summary statistics derived from individuals of European ancestries. Future investigations should  
424 extend these findings to diverse ethnic groups, particularly those that are underrepresented, to  
425 ascertain broader applicability. This necessitates the research community's commitment to  
426 embracing open science in AI and genetics. Secondly, the computational genomics statistical  
427 methods utilized in this research rely on several underlying statistical assumptions, which could  
428 potentially be violated and introduce bias. We mitigated bias by employing multiple  
429 methodologies to compute heritability, genetic correlation, and causality to address this concern.  
430 Additionally, we conducted thorough sensitivity checks, and the detailed results are provided  
431 accordingly. Additionally, our analysis was limited by the lack of individual-level genotype data  
432 from FinnGen and PGC, highlighting the need for future studies utilizing individual-level data to  
433 validate our empirical findings. Finally, our study recognizes a tradeoff between clinical  
434 interpretability and the detection of genetic associations when using AI-derived phenotypes.

435

436 **Outlook**

437 In summary, we introduced the MUTATE genetic atlas to comprehensively comprehend the  
438 genetic architecture of AI endophenotypes and chronic diseases in multi-organ science. This  
439 investigation underscores the potential of integrating AI into genetic research and supports a  
440 comprehensive approach to investigating human diseases within a multi-organ paradigm.

## 441 **STAR \* Methods**

### 442 **Method 1: GWAS summary statistics**

443 The present study solely utilized GWAS summary statistics; no individual-level data were used.  
444 We downloaded the GWAS summary statistics from three web portals for the 2024 MAEs, 521  
445 DEs from FinnGen, and 4 DEs from PGC, respectively.

### 447 **UKBB**

448 UKBB is a population-based study of approximately 500,000 people recruited from the United  
449 Kingdom between 2006 and 2010. The UKBB study has ethical approval, and the ethics  
450 committee is detailed here: [https://www.ukbiobank.ac.uk/learn-more-about-uk-  
451 biobank/governance/ethics-advisory-committee](https://www.ukbiobank.ac.uk/learn-more-about-uk-biobank/governance/ethics-advisory-committee).

452 The GWAS summary statistics for all the 2024 MAEs are publicly available at the  
453 MEDICINE knowledge portal: <https://labs-laboratory.com/medicine>, which focuses on  
454 disseminating scientific findings on imaging genetics and AI methods in multi-organ science.  
455 Specifically, among the 2024 MAEs, 2003 PSCs – at varying scales from C32 to C1024 – were  
456 structural covariance networks derived via the sopNMF method<sup>12</sup>. 9 DNEs<sup>1</sup> captured the  
457 neuroanatomical heterogeneity of four brain diseases (AD1-2, ASD1-3, LLD1-2, and SCZ1-2)  
458 using semi-supervised clustering or representation learning methods<sup>42,62,71,72</sup>. 12 multi-organ  
459 BAGs (GM, WM, FC<sup>6</sup>, multimodal brain BAGs, cardiovascular BAG, eye BAG, hepatic BAG,  
460 immune BAG, musculoskeletal BAG, metabolic BAG, pulmonary BAG, and renal BAG<sup>73</sup>) were  
461 derived from various machine learning models to quantify the individual-level deviation from  
462 typical brain aging due to various pathological effects. Detailed AI methodologies are presented  
463 in **Method 2** for the MAEs, DNEs, and BAGs. All GWASs were performed within European  
464 ancestries and using the GRCh37 human genome assembly; the GWAS model (PLINK<sup>74</sup> for  
465 linear model and fastGWA<sup>75</sup> for linear mixed-effect model), sample sizes, and covariates  
466 included are detailed in the original papers and also in **Supplementary eTable 1a**.

467 Harmonization of GWAS summary statistics across different models and consortia for  
468 various software is crucial, such as aligning the effect allele and the direction of the effect size.  
469 There's currently no established standard in the field for this process, although some advice has  
470 been proposed<sup>76</sup>. Certain software harmonizes data based on the allele frequency of the effect  
471 allele, such as the *TwoSampleMR* package<sup>77</sup> for Mendelian randomization. In our UKBB MAE  
472 GWAS summary data, we harmonized the effect allele as the alternative allele from PLINK and  
473 A1 from fastGWA and provided its corresponding allele frequency. P-value, effect sizes (e.g.,  
474 BETA value and SE), and sample sizes are indicated too. The variant identifier is based on the rs  
475 ID number, not the chromosome number and position number combination.

### 477 **FinnGen**

478 The FinnGen<sup>22</sup> study is a research project based in Finland that explores combined genetics and  
479 health registry data to understand the underlying causes and mechanisms behind various disease  
480 endpoints. It particularly emphasizes the genetic basis of diseases in the Finnish population  
481 (>500,000) by conducting extensive GWAS and analyzing large-scale genomic data in  
482 collaboration with multiple research institutions and organizations. FinnGen has generously  
483 made their GWAS results publicly available to the community for research purposes  
484 ([https://www.finnngen.fi/en/access\\_results](https://www.finnngen.fi/en/access_results)).

485 The present study used the GWAS summary statistics version R9 released to the public  
486 on May 11, 2022, after harmonization by the consortium. In the R9 release, FinnGen analyzed  
487 2269 binary and 3 quantitative endpoints from 377,277 individuals and 20,175,454 variants.  
488 Regenie<sup>78</sup> was used to run the GWAS models, including sex, age, 10 PCs, and genotyping batch  
489 as covariates. Genotype imputation was done with the population-specific SISu v4.0 reference  
490 panel. In our analysis, we concentrated solely on binary DEs with case numbers exceeding 5000  
491 to ensure adequate statistical power, given the highly imbalanced case/control ratios. As the  
492 released data were based on the GRCh38 human genome assembly, we lifted the GWAS  
493 summary statistics to the GRCh37 version for all genetic analyses. **Supplementary eTable 1b**  
494 details the included 521 DEs. More details can be found at the FinnGen website:  
495 <https://finngen.gitbook.io/documentation/v/r9/>.

496 The FinnGen team has systematically harmonized the GWAS summary data for the 521  
497 DEs involved. The alternative allele serves as the effect allele. The rsID number represents the  
498 SNP; the chromosome number and position are also shared. The data includes P-values, effect  
499 sizes, and allele frequencies for both the alternative and reference alleles.

500

### 501 **Psychiatric Genomics Consortium**

502 PGC<sup>23</sup> is an international coalition of researchers exploring the genetic underpinnings of  
503 psychiatric disorders and beyond. This collaborative effort unites scientists globally to examine  
504 and decipher extensive genomic datasets concerning various brain diseases. The primary goal of  
505 PGC involves uncovering and comprehending the genetic elements that contribute to various  
506 psychiatric disorders, such as schizophrenia, bipolar disorder, and major depressive disorder. We  
507 downloaded GWAS summary statistics from the PGC website ([https://pgc.unc.edu/for-](https://pgc.unc.edu/for-researchers/download-results/)  
508 [researchers/download-results/](https://pgc.unc.edu/for-researchers/download-results/)) and manually harmonized the data to our Mendelian  
509 randomization analyses to replicate the FinnGen findings.

510 PGC did not harmonize the GWAS summary statistics; the available data information  
511 depends on each study. **Supplementary eTable 1c** details the 4 DEs (AD, ADHD, bipolar  
512 disorder, and schizophrenia) included after the data filtering procedure. First, we ensured that the  
513 study population comprised individuals of European ancestry and, if necessary, lifted the data to  
514 the human genome build assembly GRCh37. Secondly, we excluded two studies where the allele  
515 frequency is unavailable because the *TwoSampleMR* package<sup>77</sup> requires this information to  
516 harmonize the exposure and outcome data (e.g., flip the effect allele and effect size). Thirdly, we  
517 confirmed that the GWAS summary statistics didn't overlap with UKBB data. Specifically, the  
518 AD GWAS summary data<sup>79</sup> explicitly offered a version that excluded participants from UKBB.  
519 In addition, the original dataset lacked a column for the rsID number. To deal with this, we  
520 employed a mapping approach using the chromosome number and position to the dpSNP  
521 database (version 150), which allowed us to obtain the corresponding rsID numbers. All 4 DE  
522 GWAS summary data went through the same harmonization procedure as FinnGen (**Method 3c**)

523

524

### 525 **Method 2: 2024 multi-organ AI endophenotypes**

#### 526 **(a): The 2003 patterns of structural covariance of the brain**

527 In our earlier study<sup>12</sup>, we utilized the sopNMF method on an extensive and varied brain imaging  
528 MRI dataset ( $N=50,699$ , including data from UKBB) to generate the multi-scale brain PSCs. The  
529 scale C ranges from 32 to 1024, progressively increasing by a factor of 2; 11 PSCs vanished  
530 during models.



531 Biologically, the 2003 PSCs represent data-driven structural networks that co-vary across  
532 brain regions and individuals in a coordinated fashion. Mathematically, the sopNMF method is a  
533 stochastic approximation ("deep learning-analogy") constructed and extended based on  
534 opNMF<sup>80,81</sup>. Consider an imaging dataset comprising  $n$  images, each containing  $d$  voxels. We  
535 represent the data as a matrix  $X$ , where each column corresponds to a flattened image:  $X =$   
536  $[x_1, x_2, \dots, x_n]$ ,  $X \in \mathbb{R}_{\geq 0}^{d \times n}$ . The method factorizes  $X$  into two low-rank matrices  $W \in \mathbb{R}_{\geq 0}^{d \times r}$  and  
537  $H \in \mathbb{R}_{\geq 0}^{r \times n}$ , subject to two important constraints: *i*) non-negativity and *ii*) column-wise  
538 orthonormality. More mathematical details can be referred to the original references<sup>12,80,81</sup> and  
539 **Supplementary eMethod 2a**.

#### 541 **(b): The 9 dimensional neuroimaging endophenotypes of the brain**

542 The nine DNEs captured the neuroanatomical heterogeneity of four brain diseases, including  
543 AD1-2 for AD<sup>62</sup>, ASD1-3 for autism spectrum disorder<sup>42</sup>, LLD1-2 for late-life depression<sup>71</sup>, and  
544 SCZ1-2 for schizophrenia<sup>72</sup>. The underlying AI methodologies involved two different semi-  
545 supervised clustering or representation learning algorithms: Surreal-GAN<sup>82</sup> and HYDRA<sup>83</sup>. Refer  
546 to a review for details of the semi-supervised learning<sup>84</sup>, which primarily seeks the so-called "*I-*  
547 *to-k*" mapping patterns or transformations from reference domains (like healthy controls) to  
548 target domains (such as patients).

549 Surreal-GAN<sup>82</sup> was used to derive AD1-2<sup>62</sup>. It unravels the intrinsic heterogeneity  
550 associated with diseases through a deep representation learning approach. The methodological  
551 innovation, compared to its preceptor Smile-GAN<sup>85</sup>, lies in how Surreal-GAN models disease  
552 heterogeneity: it interprets it as a continuous dimensional representation, ensures a consistent  
553 increase in disease severity within each dimension, and permits the simultaneous presence of  
554 multiple dimensions within the same participant without exclusivity. More mathematical details  
555 are presented in **Supplementary eMethod 2b**.

556 HYDRA<sup>83</sup> was employed to derive the other 7 DNEs. It utilizes a widely adopted  
557 discriminative technique, namely support vector machines (SVM), to establish the "*I-to-k*"  
558 mapping. The model extends multiple linear SVMs to the nonlinear domain by piecing them  
559 together. This approach serves the dual purpose of classification and clustering simultaneously.  
560 Specifically, it creates a convex polytope by amalgamating hyperplanes derived from  $k$  linear  
561 SVMs. This polytope separates the healthy control group from the  $k$  subpopulations within the  
562 patient group. Conceptually, each face of this convex polytope can be likened to encoding each  
563 subtype (categorical trait) or dimension (continuous trait), capturing distinctive disease effects  
564 (Refer to **Supplementary eMethod 2c**).

#### 566 **(c): The 12 biological age gaps of nine human organ systems**

567 The nine multi-organ BAGs (brain, cardiovascular, eye, hepatic, immune, musculoskeletal,  
568 metabolic, pulmonary, and renal) were derived from a previous study<sup>5</sup> that used AI to predict the  
569 chronological age of healthy individuals without chronic medical conditions: AI-predicted age –  
570 chronological age. Using a 20-fold cross-validation procedure, we applied the model for each  
571 organ system, employing a linear support vector machine. Before training each model iteration,  
572 standardization was applied to measures (excluding categorical variables) within the training set.  
573 The model was solved using sequential minimal optimization with a gap tolerance of 0.001. The  
574 support vector regression settings were adjusted for optimization, adhering to established  
575 principles in the field<sup>86</sup>.

576           Alongside the nine organ BAGs, we previously derived three multimodal brain BAGs  
577 (GM, WM, and FC-IDP) using features from gray matter (GM), white matter (WM), and  
578 functional connectivity (FC) in MRI scans<sup>6</sup>. We systematically compared four machine learning  
579 models: SVR, LASSO regression, multilayer perceptron, and a five-layer neural network. We  
580 employed nested cross-validation (CV) and included an independent test dataset<sup>87</sup> for a fair  
581 comparison across different models and MRI modalities. This process involved an outer loop CV  
582 with 100 repeated random splits: 80% for training and validation and 20% for testing. Within the  
583 inner loop, a 10-fold CV was utilized for hyperparameter tuning. Furthermore, we reserved an  
584 independent test dataset, which was kept unseen until the fine-tuning of the machine learning  
585 models<sup>88</sup> (e.g., hyperparameters for SVR) was completed.  
586

### 587 **Method 3: Genetic analyses based on GWAS summary statistics**

#### 588 **(a): The genetic architecture of the 2024 MAEs and 525 DEs**

589 Primarily, we used SBayesS<sup>39</sup> to estimate three sets of parameters that fully unveil the genetic  
590 architecture of the 2024 MAEs and 525 DEs. SBayesS is an expanded approach capable of  
591 estimating three essential parameters characterizing the genetic architecture of complex traits  
592 through a Bayesian mixed linear model<sup>89</sup>. This method only requires GWAS summary statistics  
593 of the SNPs and LD information from a reference sample. These parameters include SNP-based  
594 heritability ( $h_{SNP}^2$ ), polygenicity ( $\pi$ ), and the relationship between minor allele frequency (MAF)  
595 and effect size ( $S$ ). We used the software pre-computed sparse LD correlation matrix derived  
596 from the European ancestry by Zeng et al.<sup>39</sup>. More mathematical details can be found in the  
597 original paper from Zeng et al.<sup>39</sup>. We ran the *gctb* command<sup>89</sup> using the argument *--sbayes S*, and  
598 left all other arguments by default. When applying SBayesS to the 2025 MAEs and 525 DEs  
599 summary data, we found that 18 DEs failed to converge in the MCMC sampling, which may be  
600 due to LD differences between FinnGen and UKBB samples (the latter was used as the LD  
601 reference in SBayesS).

602           To benchmark different methods used in the field for SNP-based heritability estimates,  
603 we also employed two other methods based on GWAS summary data: *i*) LDSC<sup>28</sup> and *ii*)  
604 SumHer<sup>33</sup>. LDSC relies on the principle that the correlation between SNP effect sizes and  
605 linkage disequilibrium with neighboring SNPs can be used to estimate the proportion of  
606 heritability explained by all SNPs using GWAS summary data. For LDSC, we used the  
607 precomputed LD scores from the 1000 Genomes of European ancestry. All other parameters  
608 were set to default in the software. After merging the GWAS summary statistics, we chose the  
609 1000 Genomes reference panel for fair comparisons between the two studies and ensured that  
610 most SNPs were included in the analyses. For example, for the DE  
611 (RX\_PARACETAMOL\_NSAID), after merging with the reference panel LD, 1,171,361  
612 remained. For the first MAE (C32\_1), 1,092,510 SNPs remained after the same merging  
613 procedure. Furthermore, FinnGen didn't provide the original genotype data; they only shared the  
614 LD information via the LDstore software but did not provide the allele information.  
615 Consequently, we cannot generate in-sample LD scores using the LDSC software. Finally, a  
616 prior investigation<sup>90</sup> showcased the robustness of LDSC concerning the selection of LD  
617 reference panels – multi-ethnic European, Finnish-only, non-Finnish European from 1000  
618 Genomes Phase 3 data, and FINRISK Finnish reference panel – regarding heritability estimates  
619 in four lipid traits within a Finnish population.

620 For SumHer, we used the BLD-LDAK model, as the software suggested. BLD-LDAK  
621 stands for "Bayesian LD-adjusted Kinship," where LD-adjusted kinship refers to the calculation  
622 of genetic relatedness between individuals using information about the correlation of alleles  
623 between nearby SNPs (linkage disequilibrium). We used the software-provided tagging file,  
624 generated from 2000 white British individuals, as a reference panel suggested by the software for  
625 European ancestry groups. The HapMap3 data ([https://www.broadinstitute.org/medical-and-](https://www.broadinstitute.org/medical-and-population-genetics/hapmap-3)  
626 [population-genetics/hapmap-3](https://www.broadinstitute.org/medical-and-population-genetics/hapmap-3)) merged with the tested GWAS summary SNPs. Similarly, we  
627 ensured sufficient SNPs remained after merging with the reference panel. All other parameters  
628 were set to default. SumHer differs from LDSC in several ways: *i*) it models inflation  
629 multiplicatively, whereas LDSC uses an additive approach; *ii*) it accounts for uneven LD patterns  
630 and incorporates MAF on SNP effect; and *iii*) it utilizes a restricted maximum likelihood  
631 solver rather than regression to estimate the  $h_{SNP}^2$ .

632  
633 **(b): Genetic correlation:** We used three different methods to compute the MAE-DE pairwise  
634 ( $N=2024 \times 525=1,062,600$ ) genetic correlations ( $r_g$ ): *i*) LDSC<sup>28</sup>, *ii*) GNOVA<sup>34</sup>, and *iii*) HDL<sup>38</sup>.

635 An earlier study<sup>92</sup> highlighted the significance of selecting an appropriate LD score  
636 reference panel for genetic correlation estimates based on summary statistics. We generated the  
637 same reference panel for LD scores across the three software for a fair comparison. For LDSC,  
638 we used the precomputed LD scores from the 1000 Genomes of European ancestry provided by  
639 the software. All other parameters were set by default. To employ GNOVA, we created the LD  
640 scores utilizing the 1000 Genomes of European ancestry using the `--save-ld` argument within the  
641 `gnova.py` script. For HDL, we used the provided scripts from HDL to generate the LD scores  
642 using the same 1000 Genomes of European ancestry  
643 (<https://github.com/zhenin/HDL/wiki/Build-a-reference-panel>).

644 Through our analysis, we found that the three packages have different levels of model  
645 convergence rates, which is critical for future applications as these open-source packages claim  
646 to advance genetic research. In particular, we found that LDSC (1,062,577/1,062,600) and  
647 GNOVA (1,062,600/1,062,600) converged for most of the tested MAE-DE pairs, whereas HDL  
648 failed a substantial proportion of the analyses, leading to only 59,291 out of the 1,062,600 MAE-  
649 DE pairs (refer to the raised issue: <https://github.com/zhenin/HDL/issues/30>). Therefore, in **Fig.**  
650 **2**, we presented common significant results after Bonferroni corrections from the LDSC and  
651 GNOVA, resulting in 133 and 45 significant signals corrected on *i*) the number of MAEs and *ii*)  
652 the number of MAEs and DEs.

653  
654 **(c): Two-sample bidirectional Mendelian randomization:** We employed a bidirectional, two-  
655 sample Mendelian randomization using the *TwoSampleMR* package<sup>77</sup> to infer the causal  
656 relationships between the 2024 MAEs, 521 DEs from FinnGen, and 4 brain DEs from PGC.

657 The forward Mendelian randomization examined causality from the 2024 MAEs to the  
658 525 DEs, while the inverse analysis investigated causality from the 525 DEs to the 2024 MAEs.  
659 The *TwoSampleMR* package<sup>77</sup> applied five different Mendelian randomization methods. We  
660 presented the significant findings after the Bonferroni correction using the inverse variance  
661 weighted (IVW) estimator, verifying that the correction remained significant in at least one of  
662 the other four estimators (Egger, weighted median, simple mode, and weighted mode  
663 estimators). For the significant signals, we performed several sensitivity analyses. First, a  
664 heterogeneity test was performed to check for violating the IV assumptions. Horizontal  
665 pleiotropy was estimated to navigate the violation of the IV's exclusivity assumption<sup>93</sup> using a



666 funnel plot, single-SNP Mendelian randomization approaches, and Mendelian randomization  
667 Egger estimator. Moreover, the leave-one-out analysis excluded one instrument (SNP) at a time  
668 and assessed the sensitivity of the results to individual SNP.

669 Critically, to enhance transparency and reproducibility, we followed a systematic  
670 procedure guided by the STROBE-MR Statement<sup>94</sup> in conducting all causality analyses. This  
671 comprehensive approach encompassed the selection of exposure and outcome variables,  
672 reporting full sets of statistics, and implementing sensitivity checks to identify potential  
673 violations of underlying assumptions. First, we performed an unbiased quality check on the  
674 GWAS summary statistics. Notably, the absence of population overlapping bias<sup>29</sup> was  
675 confirmed, given that FinnGen and UKBB participants largely represent European ancestry  
676 populations without explicit overlap. For the four PGC DEs, we ensured that no UKBB  
677 participants were included in the GWAS summary data. Furthermore, all GWAS summary  
678 statistics were based on or lifted to GRCh37. Subsequently, we selected the effective exposure  
679 variables by assessing the statistical power of the exposure GWAS summary statistics in terms of  
680 instrumental variables (IVs), ensuring that the number of IVs exceeded 8 before harmonizing the  
681 data. Crucially, the function "*clump\_data*" was applied to the exposure GWAS data, considering  
682 LD. The function "*harmonise\_data*" was then used to harmonize the GWAS summary statistics  
683 of the exposure and outcome variables. This overall resulted in a smaller number (< 525 DEs or  
684 2024 MAEs) of effective exposure/outcome variables in both forward and inverse Mendelian  
685 randomization analyses, as certain GWAS summary data did not have enough IVs.

686  
687 **(d): PRS calculation:** PRS calculation used the GWAS summary statistics from the split-sample  
688 sensitivity analysis from our previous studies<sup>12,6,4,1</sup>. We established PRS weights using split1  
689 GWAS data as the base/training set, while the split2 GWAS summary statistics were used as the  
690 target/testing data. Details of the quality control (QC) procedures are shown in our previous  
691 studies<sup>12,6,4,1</sup>. Following the QC procedures, PRS for the split2 group was computed using PRS-  
692 CS<sup>45</sup>. PRS-CS infers posterior SNP effect sizes under continuous shrinkage priors using GWAS  
693 summary statistics and an LD reference panel (i.e., UKBB reference). To ascertain the most  
694 suitable PRS, we conducted a linear regression encompassing different P-value thresholds  
695 (0.001, 0.05, 0.1, 0.2, 0.3, 0.4, 0.5), while controlling for age, sex, intracranial volume (if  
696 applicable), and the forty genetic principal components. The optimal P-value threshold for PRS-  
697 MAE was determined based on the highest incremental  $R^2$ .

698 After determining the optimal model, we applied the model to the entire UKBB sample  
699 (~500k individuals). We then performed a PWAS to link the 2024 PRS-MAEs and 59 additional  
700 phenotypes (**Supplementary eTable 5**) not used to compute the PRS-MAE to avoid the circular  
701 bias<sup>46</sup>. The 59 phenotypes include cognitive scores (e.g., fluid intelligence score; Field ID:  
702 20016, mental traits (e.g., fed-up feelings; Filed ID: 1960), and lifestyle factors (e.g., tea intake;  
703 Filed ID: 1488). A linear regression was built considering the following covariates: sex (Field  
704 ID: 31), smoking status (Field ID: 20116), weight (Field ID: 21002), standing height (Field ID:  
705 50), waist circumference (Field ID: 48), age at recruitment (Field ID: 21022), and first 40 genetic  
706 principal components (Field ID: 22009).

707  
708

## 709 **Data Availability**

710 The results of the MUTATE atlas are disseminated at the MUTATE knowledge portal:  
711 <https://labs-laboratory.com/mutate>. The GWAS summary statistics for the 2024 MAEs can be  
712 accessed publicly through the MEDICINE knowledge portal: [https://labs-](https://labs-laboratory.com/medicine)  
713 [laboratory.com/medicine](https://labs-laboratory.com/medicine) and the BRIDGEPORT knowledge portal: [https://labs-](https://labs-laboratory.com/bridgeport)  
714 [laboratory.com/bridgeport](https://labs-laboratory.com/bridgeport). The GWAS summary statistics for the 521 DEs from FinnGen are  
715 publicly available at: <https://finngen.gitbook.io/documentation/v/r9/>. The GWAS summary  
716 statistics for the 4 DEs from PGC are publicly available at: [https://pgc.unc.edu/for-](https://pgc.unc.edu/for-researchers/download-results/)  
717 [researchers/download-results/](https://pgc.unc.edu/for-researchers/download-results/). The study used only GWAS summary statistics rather than  
718 individual-level data from the UK Biobank. However, the 2024 MAE GWAS data was initially  
719 derived from previous studies conducted under Application Numbers 35148 and 60698 from the  
720 UK Biobank.

## 721 **Code Availability**

722 The software and resources used in this study are all publicly available:

- 723 • *GCTB*: <https://cnsgenomics.com/software/gctb/#Overview>, SNP-based heritability,  
724 polygenicity, and MAF/effect size ratio
- 725 • *LDSC*: <https://github.com/bulik/ldsc>, SNP-based heritability and genetic correlation
- 726 • *SumHer*: <https://dougsspeed.com/sumher/>, SNP-based heritability
- 727 • *GNOVA*: <https://github.com/xtonyjiang/GNOVA>, genetic correlation
- 728 • *HDL*: <https://github.com/zhenin/HDL>, genetic correlation
- 729 • *TwoSampleMR*: <https://mrcieu.github.io/TwoSampleMR/index.html>, Mendelian  
730 randomization
- 731 • PRS-CS: <https://github.com/getian107/PRScs>, PRS
- 732 • Surreal-GAN: <https://github.com/zhijian-yang/SurrealGAN>, to derive AD1 and AD2
- 733 • HYDRA: <https://github.com/anbai106/mlni>, to derive LLD1-2, SCZ1-2, ASD1-3, and  
734 GM-, WM-, FC-BAG
- 735 • sopNMF: <https://github.com/anbai106/SOPNMF>, to derive the 2003 brain PSCs
- 736 • BioAge: <https://github.com/yetianmed/BioAge>, to derive the 9 multi-organ BAGs  
737

738 **Competing Interests**

739 None

740

741 **Authors' contributions**

742 Dr. Wen has full access to all the study data and is responsible for its integrity and accuracy.

743 *Study concept and design:* W.J

744 *Acquisition, analysis, or interpretation of data:* W.J

745 *Drafting of the manuscript:* W.J

746 *Critical revision of the manuscript for important intellectual content:* All authors

747 *Statistical analysis:* W.J

## 748 **References**

- 749 1. Wen, J. *et al.* Neuroimaging-AI Endophenotypes of Brain Diseases in the General  
750 Population: Towards a Dimensional System of Vulnerability. 2023.08.16.23294179  
751 Preprint at <https://doi.org/10.1101/2023.08.16.23294179> (2023).
- 752 2. Trubetskoy, V. *et al.* Mapping genomic loci implicates genes and synaptic biology in  
753 schizophrenia. *Nature* **604**, 502–508 (2022).
- 754 3. Kendler, K. & Neale, M. Endophenotype: a conceptual analysis. *Mol Psychiatry* **15**, 789–  
755 797 (2010).
- 756 4. Wen, J. *et al.* The Genetic Architecture of Biological Age in Nine Human Organ Systems.  
757 *medRxiv* 2023.06.08.23291168 (2023) doi:10.1101/2023.06.08.23291168.
- 758 5. Tian, Y. E. *et al.* Heterogeneous aging across multiple organ systems and prediction of  
759 chronic disease and mortality. *Nat Med* 1–11 (2023) doi:10.1038/s41591-023-02296-6.
- 760 6. Wen, J. *et al.* The genetic architecture of multimodal human brain age. *Nat Commun* **15**,  
761 2604 (2024).
- 762 7. Zhao, B. *et al.* Heart-brain connections: Phenotypic and genetic insights from magnetic  
763 resonance images. *Science* **380**, abn6598 (2023).
- 764 8. McCracken, C. *et al.* Multi-organ imaging demonstrates the heart-brain-liver axis in UK  
765 Biobank participants. *Nat Commun* **13**, 7839 (2022).
- 766 9. Nie, C. *et al.* Distinct biological ages of organs and systems identified from a multi-omics  
767 study. *Cell Reports* **38**, 110459 (2022).
- 768 10. Liu, Y. *et al.* Genetic architecture of 11 organ traits derived from abdominal MRI using  
769 deep learning. *eLife* **10**, e65554 (2021).

- 770 11. Oh, H. S.-H. *et al.* Organ aging signatures in the plasma proteome track health and disease.  
771 *Nature* **624**, 164–172 (2023).
- 772 12. Wen, J. *et al.* Genomic loci influence patterns of structural covariance in the human brain.  
773 *Proceedings of the National Academy of Sciences* **120**, e2300842120 (2023).
- 774 13. Hodson, R. Precision medicine. *Nature* **537**, S49–S49 (2016).
- 775 14. Gottesman, I. I. & Gould, T. D. The endophenotype concept in psychiatry: etymology and  
776 strategic intentions. *Am J Psychiatry* **160**, 636–645 (2003).
- 777 15. Cannon, T. D. & Keller, M. C. Endophenotypes in the Genetic Analyses of Mental  
778 Disorders. *Annual Review of Clinical Psychology* **2**, 267–290 (2006).
- 779 16. Rajpurkar, P., Chen, E., Banerjee, O. & Topol, E. J. AI in health and medicine. *Nat Med* **28**,  
780 31–38 (2022).
- 781 17. Bycroft, C. *et al.* The UK Biobank resource with deep phenotyping and genomic data.  
782 *Nature* **562**, 203–209 (2018).
- 783 18. Miller, K. L. *et al.* Multimodal population brain imaging in the UK Biobank prospective  
784 epidemiological study. *Nature Neuroscience* **19**, 1523–1536 (2016).
- 785 19. Elliott, L. T. *et al.* Genome-wide association studies of brain imaging phenotypes in UK  
786 Biobank. *Nature* **562**, 210–216 (2018).
- 787 20. Sun, B. B. *et al.* Plasma proteomic associations with genetics and health in the UK  
788 Biobank. *Nature* **622**, 329–338 (2023).
- 789 21. Dhindsa, R. S. *et al.* Rare variant associations with plasma protein levels in the UK  
790 Biobank. *Nature* **622**, 339–347 (2023).
- 791 22. Kurki, M. I. *et al.* FinnGen provides genetic insights from a well-phenotyped isolated  
792 population. *Nature* **613**, 508–518 (2023).

- 793 23. O'Donovan, M. C. What have we learned from the Psychiatric Genomics Consortium.  
794 *World Psychiatry* **14**, 291–293 (2015).
- 795 24. Buniello, A. *et al.* The NHGRI-EBI GWAS Catalog of published genome-wide association  
796 studies, targeted arrays and summary statistics 2019. *Nucleic Acids Res* **47**, D1005–D1012  
797 (2019).
- 798 25. Elsworth, B. *et al.* The MRC IEU OpenGWAS data infrastructure. 2020.08.10.244293  
799 Preprint at <https://doi.org/10.1101/2020.08.10.244293> (2020).
- 800 26. Watanabe, K. *et al.* A global overview of pleiotropy and genetic architecture in complex  
801 traits. *Nat Genet* **51**, 1339–1348 (2019).
- 802 27. Shen, L. & Thompson, P. M. Brain Imaging Genomics: Integrated Analysis and Machine  
803 Learning. *Proceedings of the IEEE* **108**, 125–162 (2020).
- 804 28. Bulik-Sullivan, B. K. *et al.* LD Score regression distinguishes confounding from  
805 polygenicity in genome-wide association studies. *Nat Genet* **47**, 291–295 (2015).
- 806 29. Sanderson, E. *et al.* Mendelian randomization. *Nat Rev Methods Primers* **2**, 1–21 (2022).
- 807 30. Bowden, J., Davey Smith, G. & Burgess, S. Mendelian randomization with invalid  
808 instruments: effect estimation and bias detection through Egger regression. *Int J Epidemiol*  
809 **44**, 512–525 (2015).
- 810 31. Open science. *Nature* **550**, 7–8 (2017).
- 811 32. Bulik-Sullivan, B. *et al.* An atlas of genetic correlations across human diseases and traits.  
812 *Nat Genet* **47**, 1236–1241 (2015).
- 813 33. Speed, D. & Balding, D. J. SumHer better estimates the SNP heritability of complex traits  
814 from summary statistics. *Nat Genet* **51**, 277–284 (2019).



- 815 34. Lu, Q. *et al.* A Powerful Approach to Estimating Annotation-Stratified Genetic Covariance  
816 via GWAS Summary Statistics. *The American Journal of Human Genetics* **101**, 939–964  
817 (2017).
- 818 35. Smith, G. D. & Ebrahim, S. ‘Mendelian randomization’: can genetic epidemiology  
819 contribute to understanding environmental determinants of disease? *Int J Epidemiol* **32**, 1–  
820 22 (2003).
- 821 36. Davey Smith, G. & Hemani, G. Mendelian randomization: genetic anchors for causal  
822 inference in epidemiological studies. *Hum Mol Genet* **23**, R89-98 (2014).
- 823 37. Pierce, B. L. & Burgess, S. Efficient design for Mendelian randomization studies:  
824 subsample and 2-sample instrumental variable estimators. *Am J Epidemiol* **178**, 1177–1184  
825 (2013).
- 826 38. Ning, Z., Pawitan, Y. & Shen, X. High-definition likelihood inference of genetic  
827 correlations across human complex traits. *Nat Genet* **52**, 859–864 (2020).
- 828 39. Zeng, J. *et al.* Widespread signatures of natural selection across human complex traits and  
829 functional genomic categories. *Nat Commun* **12**, 1164 (2021).
- 830 40. Evans, L. M. *et al.* Comparison of methods that use whole genome data to estimate the  
831 heritability and genetic architecture of complex traits. *Nat Genet* **50**, 737–745 (2018).
- 832 41. Ojavee, S. E., Kutalik, Z. & Robinson, M. R. Liability-scale heritability estimation for  
833 biobank studies of low-prevalence disease. *The American Journal of Human Genetics* **109**,  
834 2009–2017 (2022).
- 835 42. Hwang, G. *et al.* Assessment of Neuroanatomical Endophenotypes of Autism Spectrum  
836 Disorder and Association With Characteristics of Individuals With Schizophrenia and the  
837 General Population. *JAMA Psychiatry* (2023) doi:10.1001/jamapsychiatry.2023.0409.

- 838 43. Makowski, C. *et al.* Discovery of genomic loci of the human cerebral cortex using  
839 genetically informed brain atlases. *8* (2022).
- 840 44. Matoba, N., Love, M. I. & Stein, J. L. Evaluating brain structure traits as endophenotypes  
841 using polygenicity and discoverability. *Human Brain Mapping* **43**, 329–340 (2022).
- 842 45. Ge, T., Chen, C.-Y., Ni, Y., Feng, Y.-C. A. & Smoller, J. W. Polygenic prediction via  
843 Bayesian regression and continuous shrinkage priors. *Nat Commun* **10**, 1776 (2019).
- 844 46. Kriegeskorte, N., Simmons, W. K., Bellgowan, P. S. F. & Baker, C. I. Circular analysis in  
845 systems neuroscience: the dangers of double dipping. *Nat. Neurosci.* **12**, 535–540 (2009).
- 846 47. Sakaue, S. *et al.* A cross-population atlas of genetic associations for 220 human  
847 phenotypes. *Nat Genet* **53**, 1415–1424 (2021).
- 848 48. Lee, S. H. *et al.* Genetic relationship between five psychiatric disorders estimated from  
849 genome-wide SNPs. *Nat Genet* **45**, 984–994 (2013).
- 850 49. Hunter, D. J. Gene–environment interactions in human diseases. *Nat Rev Genet* **6**, 287–298  
851 (2005).
- 852 50. Wen, J. *et al.* Genetic, clinical underpinnings of subtle early brain change along  
853 Alzheimer’s dimensions. 2022.09.16.508329 Preprint at  
854 <https://doi.org/10.1101/2022.09.16.508329> (2022).
- 855 51. THE BRAINSTORM CONSORTIUM *et al.* Analysis of shared heritability in common  
856 disorders of the brain. *Science* **360**, eaap8757 (2018).
- 857 52. Smith, S. M. *et al.* An expanded set of genome-wide association studies of brain imaging  
858 phenotypes in UK Biobank. *Nat Neurosci* **24**, 737–745 (2021).
- 859 53. Walsh, B. & Lynch, M. *Evolution and Selection of Quantitative Traits*. (Oxford University  
860 Press, 2018).

- 861 54. Plackett, B. A graphical guide to ischaemic heart disease. *Nature* **594**, S3–S3 (2021).
- 862 55. Peisker, F. *et al.* Mapping the cardiac vascular niche in heart failure. *Nat Commun* **13**, 3027  
863 (2022).
- 864 56. Brundel, B. J. J. M. *et al.* Atrial fibrillation. *Nat Rev Dis Primers* **8**, 1–23 (2022).
- 865 57. Barnes, P. J. *et al.* Chronic obstructive pulmonary disease. *Nat Rev Dis Primers* **1**, 1–21  
866 (2015).
- 867 58. Holgate, S. T. *et al.* Asthma. *Nat Rev Dis Primers* **1**, 1–22 (2015).
- 868 59. Ballard, C. *et al.* Alzheimer’s disease. *The Lancet* **377**, 1019–1031 (2011).
- 869 60. Marshall, M. The hidden links between mental disorders. *Nature* **581**, 19–21 (2020).
- 870 61. Eiser, A. R. & Fulop, T. Alzheimer’s Disease Is a Multi-Organ Disorder: It May Already  
871 Be Preventable. *J Alzheimers Dis* **91**, 1277–1281 (2023).
- 872 62. Wen, J. *et al.* Genetic, clinical underpinnings of subtle early brain change along  
873 Alzheimer’s dimensions. 2022.09.16.508329 Preprint at  
874 <https://doi.org/10.1101/2022.09.16.508329> (2022).
- 875 63. Guthrie, H. *et al.* Safety, Tolerability, and Pharmacokinetics of Crenezumab in Patients  
876 with Mild-to-Moderate Alzheimer’s Disease Treated with Escalating Doses for up to  
877 133 Weeks. *J Alzheimers Dis* **76**, 967–979 (2020).
- 878 64. Sevigny, J. *et al.* The antibody aducanumab reduces A $\beta$  plaques in Alzheimer’s disease.  
879 *Nature* **537**, 50–56 (2016).
- 880 65. Congdon, E. E. & Sigurdsson, E. M. Tau-targeting therapies for Alzheimer disease. *Nat Rev*  
881 *Neurol* **14**, 399–415 (2018).
- 882 66. Jack, C. R. *et al.* Tracking pathophysiological processes in Alzheimer’s disease: an updated  
883 hypothetical model of dynamic biomarkers. *Lancet Neurol* **12**, 207–216 (2013).

- 884 67. Frisoni, G. B. *et al.* The probabilistic model of Alzheimer disease: the amyloid hypothesis  
885 revised. *Nat Rev Neurosci* **23**, 53–66 (2022).
- 886 68. Tomic, D., Shaw, J. E. & Magliano, D. J. The burden and risks of emerging complications  
887 of diabetes mellitus. *Nat Rev Endocrinol* **18**, 525–539 (2022).
- 888 69. DeFronzo, R. A. *et al.* Type 2 diabetes mellitus. *Nat Rev Dis Primers* **1**, 1–22 (2015).
- 889 70. Yang, Z. *et al.* Gene-SGAN: discovering disease subtypes with imaging and genetic  
890 signatures via multi-view weakly-supervised deep clustering. *Nat Commun* **15**, 354 (2024).
- 891 71. Wen, J. *et al.* Characterizing Heterogeneity in Neuroimaging, Cognition, Clinical  
892 Symptoms, and Genetics Among Patients With Late-Life Depression. *JAMA Psychiatry*  
893 (2022) doi:10.1001/jamapsychiatry.2022.0020.
- 894 72. Chand, G. B. *et al.* Two distinct neuroanatomical subtypes of schizophrenia revealed using  
895 machine learning. *Brain* **143**, 1027–1038 (2020).
- 896 73. Wen, J. *et al.* The Genetic Architecture of Biological Age in Nine Human Organ Systems.  
897 *medRxiv* 2023.06.08.23291168 (2023) doi:10.1101/2023.06.08.23291168.
- 898 74. Purcell, S. *et al.* PLINK: A Tool Set for Whole-Genome Association and Population-Based  
899 Linkage Analyses. *Am J Hum Genet* **81**, 559–575 (2007).
- 900 75. Jiang, L. *et al.* A resource-efficient tool for mixed model association analysis of large-scale  
901 data. *Nat Genet* **51**, 1749–1755 (2019).
- 902 76. MacArthur, J. A. L. *et al.* Workshop proceedings: GWAS summary statistics standards and  
903 sharing. *Cell Genomics* **1**, (2021).
- 904 77. Hemani, G. *et al.* The MR-Base platform supports systematic causal inference across the  
905 human phenome. *eLife* **7**, e34408 (2018).

- 906 78. Mbatchou, J. *et al.* Computationally efficient whole-genome regression for quantitative and  
907 binary traits. *Nat Genet* **53**, 1097–1103 (2021).
- 908 79. Wightman, D. P. *et al.* A genome-wide association study with 1,126,563 individuals  
909 identifies new risk loci for Alzheimer’s disease. *Nat Genet* **53**, 1276–1282 (2021).
- 910 80. Sotiras, A., Resnick, S. M. & Davatzikos, C. Finding imaging patterns of structural  
911 covariance via Non-Negative Matrix Factorization. *NeuroImage* **108**, 1–16 (2015).
- 912 81. Zhirong Yang & Oja, E. Linear and Nonlinear Projective Nonnegative Matrix  
913 Factorization. *IEEE Trans. Neural Netw.* **21**, 734–749 (2010).
- 914 82. Yang, Z., Wen, J. & Davatzikos, C. Surreal-GAN:Semi-Supervised Representation  
915 Learning via GAN for uncovering heterogeneous disease-related imaging patterns. *ICLR*  
916 (2021).
- 917 83. Varol, E., Sotiras, A. & Davatzikos, C. HYDRA: Revealing heterogeneity of imaging and  
918 genetic patterns through a multiple max-margin discriminative analysis framework.  
919 *NeuroImage* **145**, 346–364 (2017).
- 920 84. Wen, J. *et al.* Subtyping Brain Diseases from Imaging Data. in *Machine Learning for Brain*  
921 *Disorders* (ed. Colliot, O.) 491–510 (Springer US, New York, NY, 2023). doi:10.1007/978-  
922 1-0716-3195-9\_16.
- 923 85. Yang, Z. *et al.* A deep learning framework identifies dimensional representations of  
924 Alzheimer’s Disease from brain structure. *Nat Commun* **12**, 7065 (2021).
- 925 86. Chang, C.-C. & Lin, C.-J. LIBSVM: A library for support vector machines. *ACM Trans.*  
926 *Intell. Syst. Technol.* **2**, 1–27 (2011).

- 927 87. Samper-González, J. *et al.* Reproducible evaluation of classification methods in  
928 Alzheimer's disease: Framework and application to MRI and PET data. *NeuroImage* **183**,  
929 504–521 (2018).
- 930 88. Wen, J. *et al.* Convolutional neural networks for classification of Alzheimer's disease:  
931 Overview and reproducible evaluation. *Medical Image Analysis* **63**, 101694 (2020).
- 932 89. Zeng, J. *et al.* Signatures of negative selection in the genetic architecture of human complex  
933 traits. *Nat Genet* **50**, 746–753 (2018).
- 934 90. Hautakangas, H. LD Score regression for estimating and partitioning heritability of lipid  
935 levels in the Finnish population. (University of Helsinki, Helsinki, 2018).
- 936 91. Speed, D., Holmes, J. & Balding, D. J. Evaluating and improving heritability models using  
937 summary statistics. *Nat Genet* **52**, 458–462 (2020).
- 938 92. Zhang, Y. *et al.* Comparison of methods for estimating genetic correlation between  
939 complex traits using GWAS summary statistics. *Brief Bioinform* **22**, bbaa442 (2021).
- 940 93. Bowden, J. *et al.* A framework for the investigation of pleiotropy in two-sample summary  
941 data Mendelian randomization. *Stat Med* **36**, 1783–1802 (2017).
- 942 94. Skrivankova, V. W. *et al.* Strengthening the Reporting of Observational Studies in  
943 Epidemiology Using Mendelian Randomization: The STROBE-MR Statement. *JAMA* **326**,  
944 1614–1621 (2021).
- 945

946 **Acknowledgment**

947 The MULTI consortium (J.W) aims to integrate multi-organ imaging with multi-omics data to  
948 advance our understanding of human aging and disease mechanisms. We sincerely thank the UK  
949 Biobank (<https://www.ukbiobank.ac.uk/>), FinnGen (<https://www.finngen.fi/en>), and PGC  
950 (<https://pgc.unc.edu/>) team for their invaluable contribution to advancing clinical research in our  
951 field.